

**The FuGas 2.21 framework for atmosphere-ocean coupling in geoscientific models: comparing and improving algorithms for the estimates of the solubilities and fluxes of greenhouse gases and aerosols DMS**

5

Vasco M. N. C. S. Vieira<sup>1</sup>, Pavel Juras<sup>2,5</sup>, Emanuela Clementi<sup>3</sup>, Heidi Pettersson<sup>4</sup> and Marcos Mateus<sup>1</sup>.

<sup>1</sup>MARETEC, Instituto Superior Técnico, Universidade de Lisboa, Av Rovisco Pais, 1049-001 Lisboa, Portugal.

10 <sup>2</sup>DataCastor, U Svobodarny 1063/6, 190 00 Praha 9, Prague, Czech Republic.

<sup>3</sup>Istituto Nazionale di Geofisica e Vulcanologia, INGV, Bologna, Italy.

<sup>4</sup>Finnish Meteorological Institute, P.O. Box 503, FI-00101 Helsinki, Finland.

<sup>5</sup>Institute of Computer Science, Czech Academy of Sciences, Prague, Czech Republic.

15 *Correspondence to:* Vasco M. N. C. S. Vieira [vasco.vieira@tecnico.ulisboa.pt](mailto:vasco.vieira@tecnico.ulisboa.pt)

**ABSTRACT**

20

Accurate estimates of the atmosphere-ocean balances and fluxes of greenhouse gases and DMS aerosols are fundamental for geoscientific models dealing with climate change. A significant part of these fluxes occur at the coastal ocean which, although much smaller than the open ocean, is also much more heterogenic. The scientific community is becoming increasingly aware of the necessity to model the Earth at finer spatial and temporal resolutions, which also requires better descriptions of the chemical, physical and biological processes involved. The standard formulations for the gas transfer velocities and solubilities are 24 and 36 years old, respectively, and recently, new alternatives have emerged. We developed a framework congregating the geophysical processes involved which are customizable with alternative formulations with different degrees of complexity and/or different theoretical backgrounds. We propose this framework as basis for novel couplers of atmospheric and oceanographic model components. We tested it with fine resolution data from the European coastal ocean. Although the benchmark and alternative solubility formulations agreed well, their minor divergences yielded differences of many tons of greenhouse gases dissolved at the ocean surface. The transfer velocities largely mismatched their estimates, a consequence of the benchmark formulation not considering factors that were proved determinant at the coastal ocean. Climate Change research requires more comprehensive simulations of atmosphere-ocean interactions but the formulations able to do it require further calibration and validation.

35

Keywords: solubility, transfer velocity, Henry constant.

## 1 Introduction

Earth-System as well as Regional models are ensembles of inter-connected components, namely the land, ocean, atmosphere and cryosphere. The exchange of information between each pair requires specific couplers that are also responsible for the estimation of geophysical processes specific to their physical interfaces. In this work we focus on the coupling between the atmospheric and the oceanographic components, and on the estimation of the air-water fluxes of greenhouse gases ~~and aerosols~~. In order to test and compare different algorithms and degrees of complexity, we developed a framework allowing to set specific customizations. Furthermore, this framework is able to automatically select simpler algorithms in particular locations where the lack of data does not allow using more comprehensive formulations. The framework can be applied to estimate the air-water fluxes of any gas on the atmosphere, including DMS, by selecting the respective constants. The solubility constants are provided by Sarmiento and Gruber (2013) or Sander (2015). The Code and Data Availability section has the link to the software, data and videos.

Because the oceans can act as sinks or sources of greenhouse gases and dimethyl sulfide (DMS) aerosols to the atmosphere, the dynamics of their gas exchanges are fundamental for Earth's climate. The open ocean is generally believed to uptake CO<sub>2</sub> from the atmosphere, despite the observed seasonal, inter-annual and regional variability. In the sub-polear regions the solubility pump retrieves large amounts of greenhouse gases from the atmosphere and transports them to the deep ocean. On the other hand, the balances and fluxes of CO<sub>2</sub>, CH<sub>4</sub>, N<sub>2</sub>O and DMS at the coastal oceans' surface are very heterogenic due to factors like upwelling, plankton productivity and continental loads. Earth-System Models (ESM) and marine biogeochemistry have difficulties simulating these processes na their inherent variability. Constrained by computational demands, they usually simulate the biosphere at decadal and centennial time-scales with daily intervals and spatial resolutions of hundreds to one thousand kilometres. (see Such are the cases of ESM applications by the Intergovernmental Panel on Climate Change (IPCC), Max Planck Institute (MPI) or Centro Euro-Mediterraneo sui Cambiamenti Climatici (CMCC). Hand-in-hand with the low resolution for space and time, Constrained by calculus demands, they estimate the atmosphere-ocean gas fluxes from simpler formulations that disregard the complexity of processes more recently unveiled at the coastal ocean. The generalization by Wanninkhof (1992), relying on wind speed ( $u_{10}$ ) as the sole driver of transfer velocity, is the standard in current ESM at coarse resolutions. Alternatively, ~~the~~ regional oceanographic numerical lab MOHID allows the user to choose between the air-water gas exchange formulations proposed by Carini et al. (1996) or ~~and~~ Raymond and Cole (2001), only accounting for  $u_{10}$ , or by Borges et al. (2004), also accounting for current drag with the bottom. These are empirical formulations best fitting low wind data collected from estuaries. There are many other simpler formulations estimating the air-water gas exchange considering a few factors that were determinant for that specific set of environmental conditions and optimizing the adjustment to their specific data used in their calibration (see the list of available formulations in the software settings). However, ~~But~~ modelling the coastal oceans with fine resolution requires an algorithm that, whatever the local conditions, is always able to forecast with improved accuracy due to its enhanced representation of the multitude of processes potentially present. Developing such algorithm demands for a framework able to be updated with the best formulation for each of the mediator processes involved.

75 | The [Flux of Gases \(FuGas\) version 2.24](#) is an upgrade of the framework by Vieira et al. (2013) congregating  
several of the geophysical processes involved in the air-water gas exchanges, and where each process can be simulated  
by one formulation chosen from an extensive list. It includes 529 alternative formulations to account for such factors as  
solubility, wind or current mediated turbulence, atmospheric stability, sea-surface roughness, breaking waves, air and  
water viscosities, temperature and salinity. We use [this framework FuGas 2.4](#) to compare between the estimations of  
80 | the solubilities and fluxes of greenhouse gases using the ESM standards and recent alternative formulations. First, we  
tested with field data from the Baltic Sea. Then, we coupled the Weather Research and Forecasting (WRF) atmospheric  
model to the WaveWatch III (WW3) - NEMO oceanographic model using simulated data from the European coastal  
ocean. The ~~calculations were~~ [vectorized and parallelized](#) for improved computational speed.

## 85 | 2 Methods

Air-water gas fluxes result from the interaction of two factors: (i) the unbalance between the gas concentrations in the  
air and in the water sets the strength and direction of the flux, and (ii) the resistance the medium does for being crossed  
by the flow. The traditional formulation estimates the flux from  $F = k_w \cdot k_{Hcp} \cdot \Delta p_{gas}$ , in units of  $\text{mol} \cdot \text{m}^{-2} \cdot \text{s}^{-1}$ . ~~The  $\Delta p_{gas}$  is the~~  
~~difference between air and water gas partial pressures (atm).~~ The  $k_{Hcp}$  is the Henry's constant for the gas solubility in  
90 | its  $C_w/p_a$  form ( $\text{mol} \cdot \text{m}^{-3} \cdot \text{atm}^{-1}$ ), where  $p_a$  is its air partial pressure (atm) and  $C_w$  its concentration in the water ( $\text{mol} \cdot \text{m}^{-3}$ ).  
[Sander \(2016\) provided the  \$k\_{Hcp}\$  in units of  \$\text{mol} \cdot \text{L}^{-1} \cdot \text{atm}^{-1}\$ , and thus conversion was required. The  \$\Delta p\_{gas}\$  is the difference](#)  
[between air and water gas partial pressures \(atm\) i.e.  \$pX\_a - pX\_w\$ . In this form a positive flux represents uptake by the](#)  
[ocean. The  \$pX\_a\$  must be corrected for the partial pressure of water vapour considering saturation over the sea-surface:](#)  
 [\$pX\_{moist} = \(1 - p\_{H\_2O}/P\)p\_{dry}\$ . This conversion is detailed in section \(2.1\) below.](#) The  $k_w$  is the transfer velocity of gases across  
95 | the sub-millimetrically thick water surface layer in  $\text{m} \cdot \text{s}^{-1}$  although usually plotted in  $\text{cm} \cdot \text{h}^{-1}$ . [For mildly soluble gases the](#)  
[airside resistance is not negligible. In these cases, ~~the alternative~~ double layer model \(Liss and Slater, 1974\) estimates](#)  
the flux taking into consideration both the water-side and air-side sub-millimetrically thick surface layers and thus,  $F =$   
 $K_w(C_a/k_H - C_w) = K_a(C_a - C_w \cdot k_H)$ . The  $C_a$  and  $C_w$  are the concentrations of the gas in air and water given in  $\text{mol} \cdot \text{m}^{-3}$  and the  
100 |  $k_H$  is Henry's constant in its equivalent dimensionless quantity ( $C_a/C_w$ ). The transfer velocity is ~~averaged overestimated~~  
~~from~~ both layers ~~from~~  $K_w = (1/k_w + 1/(k_H \cdot k_a))^{-1}$  or its equivalent  $K_a = (k_H/k_w + 1/k_a)^{-1}$ .

### 2.1 Solubility

Sarmiento and Gruber (2013) compiled the algorithm for the  $k_{Hcp}$  dependence on temperature and salinity provided by  
Weiss (1974) and Weiss and Price (1980). We converted it to its corresponding dimensionless  $k_H$  preserving the  
105 | constants required to estimate Bunsen's solubility coefficient  $\beta$ . This formulation accounted for fugacity ( $f$ ) of non-ideal  
gases (Eq. 1) and corrected the gas partial pressure for moisture effects from the expression  $p_{moist} = (1 - p_{H_2O}/P)p_{dry}$   
considering water vapour saturation over the sea-surface (Eq. 2).  $P$  is air pressure (atm),  $T_w$  is water temperature (K),  $S$   
is salinity (‰),  $p$  is the gas partial pressure (atm),  $R$  is the ideal gas law constant ( $\text{Pa} \cdot \text{m}^3 \cdot \text{mol}^{-1} \cdot \text{K}^{-1}$ ),  $V_m$  is the molar  
volume of the specific gas (22.3 for  $\text{CO}_2$  and  $\text{CH}_4$ , and 22.2432 for  $\text{N}_2\text{O}$ ) and  $V_{ideal} = 22.4136 \text{ mol} \cdot \text{L}^{-1}$  is the molar  
110 | volume of ideal gases. Solubility coefficients were estimated from the Virial expansion (Eq. 3), where  $B$  was  $\beta$  or  $\beta/V_m$ ,  
depending on which gas it was applied to (Table 3.2.2 in Sarmiento and Gruber (2013)). Our software automatically  
detected the gas from the  $a_i$  coefficient. When  $B = \beta$  the  $k_H$  was estimated from Eq. (4). When  $B = \beta/V_m$  the  $k_H$  was  
estimated from Eq. (5).

$$115 \quad f = \exp\left(\frac{101.325P(V_m - V_{ideal})}{RT_w}\right) \quad (1)$$

$$\log\frac{p_{H_2O}}{P} = 24.4543 - 67.4509\left(\frac{100}{T_w}\right) - 4.8489\ln\left(\frac{T_w}{100}\right) - 0.000544S \quad (2)$$

$$\log(B) = a_1 + a_2\frac{100}{T_w} + a_3\log\frac{T_w}{100} + a_4\left(\frac{T_w}{100}\right)^2 + S \cdot \left(b_1 + b_2\frac{T_w}{100} + b_3\left(\frac{T_w}{100}\right)^2\right) \quad (3)$$

$$k_H = \left(1 - \frac{p_{H_2O}}{P}\right) \frac{101.325V_m}{RT_w\beta f} \quad (4)$$

$$k_H = \frac{101.325}{RT_w\beta f} \quad (5)$$

120

Johnson (2010) developed an algorithm from an alternative chemistry background. It accounts for the effects of temperature and salinity taking into consideration the molecular and thermodynamic properties of the water, its solutes and the specified gas, but disregarding the non-ideal behaviour of the gases and moisture. His formulation was developed from the compilation by Sander (2015) (although available in the web since 1999) of the  $k_{Hcp}$  for nearly all gases in the atmosphere at 25° C (298.15 K) and 0 ppt. Then, equation (6) converted the  $k_{Hcp}$  to  $k_H$  at a given temperature and 0 ppt salinity. The term  $-\Delta_{soln}H/R$  reflected the temperature (in Kelvin) dependence of solubility, having a value of 2400 for CO<sub>2</sub>, 1700 for CH<sub>4</sub> and 2600 for N<sub>2</sub>O. The correction to a given salinity (Eq. 7) relied on the empirical Setschenow constants ( $K_s = \theta \cdot \log V_b$ ) reporting the effect of electrolytes salting-out gases proportionally to their liquid molar volume at boiling point ( $V_b$ ). The  $V_b$  was estimated using the additive Schroeder method, whereas  $\theta$  was estimated from Eq.8 using a provisional  $k_{H\#} = 0.0409/k_{Hcp}$ .

130

$$k_{H,0} = \frac{12.1866}{P \cdot T_w \cdot k_{H,cp} \cdot e^{\frac{-\Delta_{soln}H}{R} \left(\frac{1}{T_w} - \frac{1}{298.15}\right)}} \quad (6)$$

$$k_H = k_{H,0} \cdot 10^{K_s S} \quad (7)$$

135

$$\theta = 7.33532 \cdot 10^{-4} + 3.39615 \cdot 10^{-5} \cdot \log(k_{H\#}) - 2.40888 \cdot 10^{-6} \cdot \log(k_{H\#})^2 + 1.57114 \cdot 10^{-7} \cdot \log(k_{H\#})^3 \quad (8)$$

140

The mismatches between both algorithms lead to differences in the estimates of greenhouse gases dissolved in the first meter below the ocean surface, which were calculated from  $\Delta \text{ton}^{-1} \cdot 121 \text{ km}^{-2} = 11^2 \cdot \Delta s \cdot p_{\text{gas}} \cdot P \cdot 101325 \cdot M_g / (10^9 \cdot R \cdot T)$ . The  $\Delta s$  was the difference in the solubilities estimated by both algorithms and converted to the  $C_w/C_a$  form. Hence,  $\Delta s = 1/k_{H\#Sar13} - 1/k_{H\#Joh10}$ , and because  $C_a$  was equal among them, the  $\Delta s = (C_w^{Joh10} - C_w^{Sar13})/C_a$ . This difference of  $\text{mol} \cdot \text{m}^{-3}$  of gas in the water per  $\text{mol} \cdot \text{m}^{-3}$  of gas in the air at each cell was averaged over the 66 h time interval. In order to convert from mols to grams in the water we multiplied by the molar mass of the specific gas ( $M_g$ ), which is 44.01 for CO<sub>2</sub>, 16.043 for CH<sub>4</sub> and 44.013 for N<sub>2</sub>O. Then, we divided by  $10^6$  to convert from grams to tons. We still needed to

145 estimate  $C_a$  from the atmospheric pressure (P) and the partial pressure ( $p_{gas}$ ) of  $CO_2$ ,  $CH_4$  or  $N_2O$ , 390 ppm, 1.75 ppm  
and 0.325 ppm respectively (EPA, 2015), assuming that they were approximately uniform all over the atmospheric  
surface boundary layer (SBL). Using the ideal gas law, we divided by R and T (in Kelvin), multiplied by 101325 to  
convert Pascal to atm and divided by  $10^6$  to re-scale from ppm to unity. Finally, we multiplied by  $(11 \text{ km})^2$  to have the  
total difference in mass dissolved in the first meter below the surface of 11 km wide cells.

## 150 2.2 Transfer velocity

The available algorithms consider that the rate at which gases cross the sea-surface is basically set by the turbulence upon it. E.g. wind drag, wave breaking, currents and rain promote turbulence. The water viscosity, set by temperature and salinity and enhanced by the presence of surfactants, antagonizes turbulence. Figure 1 in the work by Wanninkhof et al. (2009) clarifies how some of these processes interact. With all these forcings, it becomes difficult to develop an algorithm that estimates the transfer velocity accurately. The literature has many of them, either fitted to specific surface conditions or rougher generalizations, focusing on different factors and relying in different theoretical backgrounds. The simpler ones rely on the wind velocity 10m above the sea-surface ( $u_{10}$ ). Among them, the formulation by Wanninkhof (1992) (henceforth also mentioned as ‘Wan92’) became the standard used in ESM and satellite data processing (equation 9a,b). It further considers the Schmidt number of the water ( $Sc_w$ ) related to viscosity and with its exponent reflecting the surface layer’s rate of turbulent renewal. Under low winds, and ~~the temperature dependent transfer velocity of  $CO_2$  is~~ chemically enhanced ~~ment~~ due to  $CO_2$ -reaction with water ( $\alpha_{Ch}$ ) and scales with temperature.

$$k_w = (\alpha_{Ch} + 0.31 \cdot u_{10}^2) \left(\frac{Sc_w}{660}\right)^{-0.5} \quad (9a)$$

$$\alpha_{Ch} = 2.5 \cdot (0.5246 + 0.0162T_w + 0.000499T_w^2) \quad (9b)$$

165 Other simple empirical formulations based only on  $u_{10}$  (Carini et al., 1996; Raymond and Cole, 2001), or also accounting for current drag with the bottom (Borges et al., 2004), used data collected in estuaries under low wind conditions. However, modelling the coastal ocean at finer resolutions requires an enhanced representation of the multitude of processes involved. Hence, we updated the framework by Vieira et al. (2013), with the  $k_w$  being decomposed into its shear produced turbulence ( $k_{wind}$ ) and bubbles from whitecapping ( $k_{bubble}$ ) forcings (Asher and Farley, 1995; Borges et al, 2004; Woolf, 2005; Zhang et al., 2006). The effect of currents was disregarded at this stage (Eq. 10).  $Sc_w$  was determined from temperature and salinity following Johnson (2010):

$$175 \quad k_w = (\alpha_{Ch} + k_{bubble} + k_{wind} + k_{current}) \cdot (600/Sc_w)^{0.5} \quad (10)$$

The formulation by Zhao et al. (2003), merged  $k_{wind}$  into  $k_{bubble}$  (Eq. 11a) using the wave breaking parameter ( $R_B$  given by Eq. 11b). The  $u_*$  is the friction velocity i.e, the velocity of wind dragging on the sea-surface, and  $f_p$  is the peak angular frequency of the wind-waves. The kinematic viscosity of air ( $\nu_a$ ) was estimated from Johnson (2010). This solution used the wave field as a proxy for whitecapping that increased transfer velocity with wind-wave age. However, it simultaneously used the wave field as a proxy for the sea-surface roughness that increased transfer velocity from wind-drag over steeper younger waves (through the WLLP estimation of  $u_*$  explained in a section below).

$$k_{\text{bubble}} = 0.1315 \cdot R_B^{0.6322} \quad (11a)$$

$$185 \quad R_B = \frac{u_*^2}{2\pi f_p v_a} \quad (11b)$$

190 A more comprehensive solution split the two drives of transfer velocity (Woolf, 2005; Zhang et al., 2006):  $k_{\text{wind}}$  for the transfer mediated by the turbulence generated by wind drag (Eq. 12, [taken from](#)) (Jähne et al., 1987) and  $k_{\text{bubble}}$  for the transfer mediated by the bubbles generated by breaking waves (Eq. 13) ([Zhang et al., 2006](#)).  $B$  is Bunsen's solubility coefficient estimated for the local sea-surface conditions.  $W=3.88 \times 10^{-7} R_B^{1.09}$  is the whitecap cover requiring the  $R_B$  estimated from [Eq. \(11b\)](#),  $V=4900$ ,  $e=14$  and  $n=1.2$ .

$$k_{\text{wind}} = 1.57 \cdot 10^{-4} \cdot u_* \quad (12)$$

$$195 \quad k_{\text{bubble}} = \frac{WV}{B} \left[ 1 + (e \cdot B \cdot Sc_w^{-1/2})^{-1/n} \right]^{-n} \quad (13)$$

200 These formulations required friction velocity ( $u_*$ ), which was estimated from the Wind Log-Linear Profile (WLLP: Eq. 14) accounting for wind speed at height  $z$  ( $u_z$ ), atmospheric stability of the surface boundary layer (through  $\psi_m$ ) and sea-surface roughness (through the roughness length  $z_0$ ). The  $\kappa$  is von Kármán's constant. [Historically, the WLLP originated from the Monin-Obukhov Similarity Theory \(Monin and Obukhov, 1954; Stull, 1988\).](#)

$$u_* = \frac{u_z \kappa}{\ln(z) - \ln(z_0) + \psi_m(z, z_0, L)} \quad (14)$$

205 Roughness length ( $z_0$ ) is the theoretical minimal height (most often sub-millimetrical) at which wind speed averages zero. It is dependent on surface roughness and often used as its index. It is more difficult to determine over water than over land as there is a strong bidirectional interaction between wind and sea-surface roughness. Taylor and Yelland (2001) proposed a dimensionless  $z_0$  dependency from the wave field, increasing with the wave slope (Eq. 15). [Here,  \$H\_s\$  is the significant wave height and  \$L\_p\$  is the peak wave period.](#) Due to the bidirectional nature of the  $z_0$  and  $u_*$  relation, we also tested an iterative solution (iWLP) where Eq.15 was used as a first guess for the  $z_0$  and Eq.14 for its subsequent  $u_*$ . A second iteration re-estimated  $z_0$  from the COARE 3.0 (Fairall et al.; 2003) adaptation of the Taylor and Yelland (2001) formulation, which added a term for smooth flow (Eq. 16), and  $u_*$  again from Eq.14. Applying four iterations were enough for an excellent convergence of the full data array. [Irrespective of the WLLP or iWLP algorithm, the coefficients proposed by Taylor and Yelland \(2001\) applied to our data sometimes yielded incredibly high and unreal  \$z\_0\$  leading to absurdly high  \$u\_\*\$  and  \$k\_w\$ . To prevent this bias we imposed a maximum roughness length  \$z\_{0,\text{max}}=0.01\$  m.](#)

$$215 \quad \frac{z_0}{H_s} = 1200 \cdot \left( \frac{H_s L_p}{L_p} \right)^{4.5} \quad (15)$$

$$z_0 = 1200 \cdot H_s \left( \frac{H_s}{L_p} \right)^{4.5} + \frac{0.11 v_a}{u_*} \quad (16)$$

220 Atmospheric stability characterized the tendency of the surface boundary layer (SBL) to be well mixed (unstable SBL  
with  $\psi_m < 0$ ) or stratified (stable SBL with  $\psi_m > 0$ ). The  $\psi_m$  was inferred from the ‘bulk Richardson number’ ( $Ri_b$ ; Eq.  
17), weighting the air vertical heat gradient and kinetic energy, and its estimation required the air virtual potential  
temperature ( $T_v$ ), in its turn, estimated from air temperature ( $T$  in °C), air pressure ( $P$  in atm), and humidity  
225 (dimensionless) and the gravitational acceleration constant ( $g$ ). Grachev and Fairall (1997) estimated  $T_v = T_p(1 + 0.61q)$ ,  
where  $T_p$  is the air potential temperature and  $q$  the observed specific humidity (Grachev and Fairall, 1997) or from  
Stull (1988) estimated  $T_v = T_p(1 + 0.61r_{sat} \cdot h_r + r_l)$ , where  $r_{sat}$  is the water vapour mixing ratio at saturation,  $h_r$  is the  
observed relative humidity and  $r_l$  the observed liquid water mixing ratio (Stull, 1988).  $T_p$  (in °C) was estimated from  $T_p$   
 $= T_k(1000/(1013.25P))^{0.284}$ , where  $T_k$  is temperature (Kelvin). The  $r_{sat} = 0.622e_{sat}/(101.32501P - e_{sat})$  and the  $\ln(e_{sat}) =$   
 $\ln(0.61078 + 17.2694T/(T_k - 35.86))$ . -Alternatively, Lee (1997) estimated the  $Ri_b$  directly the use of from the air potential  
230 temperature neglecting humidity (Lee, 1997). The wind velocity ( $u_z$ ), temperature ( $T_z$ ), pressure ( $P_z$ ) and humidity  
( $q_z$ )  $z$  meters above sea-surface were given by the WRF second level. The wind velocity at  $z_0$  ( $u_0$ ) was set to the  
theoretical  $u_0 = 0$ . Temperature at the height of 0 m ( $T_0$ ) was given by the SST (Grachev and Fairall, 1997; Fairall et al.,  
2003; Brunke et al., 2008) without rectification for cool-skin and warm-layer effects due to the lack of some required  
variables. Yet, these effects tend to compensate each other (Brunke et al., 2008; Fairall et al., 1996; Zeng and Beljars,  
235 2005). Air pressure at 0 m ( $P_0$ ) was given by the WRF at the lower first level (at roughly 0 m). Humidity at 0 m ( $q_0$ )  
was set to the saturation level at  $P_0$  and  $T_0$  using  $q = r_{sat}/(1 + r_{sat})$  (Grachev and Fairall, 1997). The  $Ri_b$  was used to estimate the  
length  $L$  from the Monin-Obukhov’s similarity theory, a discontinuous exponential function tending to  $\pm \infty$  when  $Ri_b$   
tends to  $\pm 0$  and tending to  $\pm 0$  when  $Ri_b$  tends to  $\pm \infty$ .  $Ri_b$  and  $L$  were used to estimate  $\psi_m$  following Stull (1988) or Lee  
(1997) algorithms.

240

$$Ri_b = \frac{g \Delta T_v F \Delta z_l}{T_v F u_z^2}$$

(17)

245  $CO_2$  is mildly soluble with a  $K_H = 1.17$  for pure water at 25 °C. Its transfer velocity is limited by the molecular crossing  
of the water-side surface layer.  $CH_4$  is much less soluble with a  $K_H = 31.5$  for pure water at 25 °C. The transfer  
velocity of mildly soluble gases, besides taking into consideration the molecular crossing of the water-side surface  
layer, should also take into consideration the molecular crossing of the air-side surface layer (Liss and Slater, 1974,  
Wanninkhof et al., 2009; Johnson, 2010). We compared between the use of the traditional single layer model and the  
250 double layer “thin film” model (Liss and Slater, 1974; Johnson, 2010; Vieira et al., 2013), the later requires estimating the  
air-side transfer velocity ( $k_a$ ) estimated from the COARE formulation as in Eq. 18 (Jeffrey et al., 2010).  $CD$  is the drag  
coefficient and  $Sc_a$  the Schmidt number of air, which were determined for a given temperature and salinity following  
Johnson (2010).

255

$$k_a = \frac{u_*}{13.3 \cdot Sc_a^{1/2} + CD^{1/2} - 5 + \frac{\log(Sc_a)}{2\kappa}} \quad (18)$$

### 2.3 Validation with field data

The field sampling occurred from the 22<sup>nd</sup> of May 2014 to the 26<sup>th</sup> of May 2014 using the atmospheric tower at Östergarnsholm in the Baltic Sea (57° 27' N, 18° 59' E), the Submersible Autonomous Moored Instrument (SAMI-CO<sub>2</sub>) 1 km away and the Directional Waverider (DWR) 3.5 km away, both south-eastward from the tower (see e.g. Högström et al. (2008) and Rutgersson et al. (2008) for detailed description of the sites). The air-water CO<sub>2</sub> fluxes measured by eddy-covariance were smoothed over 30 min bins and corrected according to the Webb-Pearman-Leuning (WPL) method (Webb et al., 1980). We used only the fluxes for which the wind direction set the SAMI-CO<sub>2</sub> and DWR in the footprint of the atmospheric tower (90° < wind direction < 180°). The DWR measured temperatures at 0.5 m depth, taken as representative for the sea-surface. Salinity was obtained from the Asko mooring data provided by the Baltic In-Situ Near-Real-Time Observations available in Copernicus Marine catalogue. We applied this data set to the single processing ~~software~~ ensemble of the FuGas 2.2.1 in order to test which algorithms provide better approximations to reality.

#### 2.4 Retrieving and processing Level 4 data ~~Atmosphere-ocean coupler~~

The atmospheric model was the standard operational application of the WRF by Meteodata.cz, with 9 km and 1 h resolutions. Air temperature 'T' (°C), pressure 'P' (atm), U and V components of wind velocity (m·s<sup>-1</sup>), water vapour mixing ratio 'Q' (scalar) and height 'h' (m), were retrieved at the two lowest levels within the ~~atmospheric surface boundary layer (SBL)~~. The vertical thickness of the WRF horizontal layers varied with space and time. Over the ocean, the two lowest levels occurred roughly at 0 m and 12 m heights. The WRF output decomposes height, temperature and pressure into their base level plus perturbation values.

Sea-surface temperature (SST) and salinity (S) were estimated by the NEMO modelling system provided in the MyOcean catalogue with 1/12° and 1 day resolutions. The WW3 wave field data for the Mediterranean Sea was supplied by ~~the Istituto Nazionale di Geofisica e Vulcanologia (INGV)~~ using the WW3-NEMO modelling system at 0.0625° and 1 h resolutions (Clementi, 2013), and for the North Atlantic by Windguru at roughly 0.5° and 3 h resolutions. The variables included significant wave height 'H<sub>s</sub>' (m) and peak frequency 'f<sub>p</sub>' (rad·s<sup>-1</sup>) for wind sea i.e., disregarding swell. A few aspects did not correspond to the ideal data format for atmosphere-ocean coupling, and required further calculations: (i) The peak wave length 'L<sub>p</sub>' (m) was estimated from the peak frequency assuming the deep-water approximation:  $L_p = 2\pi g / f_p^2$ , where g is the gravitational acceleration constant; (ii) the Windguru data did not provide wind sea component ~~(where (and) when)~~ the wind was too low. For these missing cases were attributed the lowest H<sub>s</sub> and L<sub>p</sub> simulated everywhere else; (iii) the Windguru and the INGV data overlapped along the Iberian shores, in which case the INGV was given a 2:1 weight over the Windguru data.

The WRF and WW3-NEMO ~~emo~~ outputs were retrieved for the European shores from the 24<sup>th</sup> of May 2014 at 06h to the 27<sup>th</sup> of May 2014 at 00 h. All variables were interpolated to the same 0.09° grid (roughly 11 km at Europe's latitudes) and 1 h time steps. This resulted in a data set with 17 variables × 41776 locations × 66 time instances, that occupied ~~over~~nearly 1Gb ram memory (with another 1Gb taken by the software). To optimize the computations, the ~~calculations~~ ~~were~~ first vectorized and then parallelized using the Single Program Multiple Data (spmd) programming strategy. Hence, in the FuGas 2.1 multiple processing ~~software~~ ensemble, ~~(supplied in the interactive discussion of this report)~~, the variables were first organized in matrices with locations along the 1<sup>st</sup> dimension and time along the 2<sup>nd</sup>. Running the ~~calculations~~ applying matrix algebra to the whole data set, by itself represented an



improved speed of several orders of magnitude. Furthermore, the spmd replicated the data, split the replicates into n approximately equal-sized arrays, and distributed their calculations among the n available cpu cores, which represented an extra improvement of computational speed. However, it also bared computational costs:

(i) ~~(i)~~ invoking the parallel processing toolbox was time consuming,

(ii) ~~(ii)~~ replicating over 1Gb ram was time consuming,

(iii) ~~(iii)~~ once when running the calculations with other programs on the background us, the 4Gb ram memory was soon exhausted. Thereafter, the use of virtual memory in the hard-disk, which stalled enormously the calculations. To prevent it the following actions were implemented,

(iv) Programs like the antivirus, backup tools, Office, Skype, Dropbox, etc were shut down in the Task Manager,

(v) ~~(iv)~~ to avoid it, the spmd were split into several sequential code blocks and in-between the variables no longer necessary were deleted. This spmd fragmentation was time consuming.

In conclusion, there is no perfect solution for ~~calculus~~ parallel computingization, and although spmd is the best strategy available for this task, its application needs to be carefully programmed according to the data and hardware characteristics. Optimizing the data management was one fundamental improvement between the 2.1 and the 2.2

versions of the FuGas. The simulations of the European coastal ocean no longer exhausted the ram memory and did not even use more than 70% of it (using above 90% becomes critical). Consequently, the computation time improved from  $\approx 12$  min to  $\approx 4$  min.

### 3 Results

~~The Both~~ solubility formulations were ~~test~~ compared simulating ~~in~~ the range of environmental conditions commonly found in nature:  $T_w$  ranged from 4°C to 30°C at 1°C intervals while  $S$  ranged from 0 ppt to 36 ppt at 1 ppt intervals.

The ~~met~~ ratio between the solubilities estimated by each formulation (i.e.  $k_{H, \text{Joh10}}/k_{H, \text{Sar13}}$ ) showed better how much the ~~seir~~ estimates could diverge (Fig. 1). Afterwards, both formulations were applied to the conditions data

~~from~~ observed at the European coastal ocean during the experiment. Their ~~estimated~~ solubilities were compared from

~~their ratio~~ applying the previous metrie averaged over the 66 h time interval using the geometric mean (Fig. 1). From the 24<sup>th</sup> to the 26<sup>th</sup> May the water temperature at the ocean surface changed significantly and there were large fresh water inputs from the Black Sea and the Baltic Sea (Video 1). The widest divergences were up to 4.5% in the CO<sub>2</sub> solubility estimates associated to cooler waters, 5.8% in the CH<sub>4</sub> solubility estimates associated to both temperature extremes, and 2.1% in the N<sub>2</sub>O solubility estimates associated to cooler and less saline waters (Fig. 1). ~~These mismatches lead to large~~

~~differences in the estimates of greenhouse gases dissolved in the first meter below the ocean surface (Fig. 2). These differences summed to  $3.86 \times 10^6$  ton of CO<sub>2</sub>, 880.7 ton of CH<sub>4</sub> and 401 ton of N<sub>2</sub>O. Because the bias of N<sub>2</sub>O changed from positive to negative with location, the overall bias was 163 ton. These differences were estimated from  $\Delta \text{ton} \cdot \text{m}^{-2} \cdot 121 \text{ km}^2 = 11^2 \cdot \Delta s \cdot p_{\text{gas}} \cdot P \cdot 101325 \cdot M_a / (10^9 \cdot R \cdot T)$ , where  $\Delta s$  was the difference in the solubility estimated by either algorithm in its  $C_w/C_a$  form at each 11 km wide cells and averaged over the 66 h time interval.  $M_a = 28.97$  was the air molecular mass and  $p_{\text{gas}}$  the atmospheric partial pressure of CO<sub>2</sub>, CH<sub>4</sub> or N<sub>2</sub>O, 390 ppm, 1.75 ppm and 0.325 ppm respectively (EPA, 2015), assuming that they were approximately uniform all over the atmospheric SBL. Integrated over space, these differences summed to  $1.17 \times 10^5$  ton of CO<sub>2</sub>, 7374.5 ton of CH<sub>4</sub> and 25.1 ton of N<sub>2</sub>O.~~

During the Baltic Sea sampling at the Östergarnsholm site the observed  $\Delta$ ppm varied within 120 and 270, well below the limit for a 25% error in the flux estimates as reported by Blomquist et al. (2014) for our IRGA model, the LI-

335 ~~COR LI-7500. Even so, These differences summed to  $3.86 \times 10^6$  ton of  $\text{CO}_2$ , 880.7 ton of  $\text{CH}_4$  and 401 ton of  $\text{N}_2\text{O}$ . Because the bias of  $\text{N}_2\text{O}$  changed from positive to negative with location, the overall bias was 163 ton.~~

340 The  $k_w$  estimated from the E-C measurements presented a systematic bias. To detect its source, the difference ( $\Delta k_w$ ) between the  $k_w$  estimated from the E-C measurements and the one estimated from the Wan92 formulation was compared to the potential sources of bias. Besides well correlated with  $u_{10}$  ( $r=0.55$ ), the  $\Delta k_w$  was also well correlated with the relative humidity ( $r=0.7$ ) and with the first ( $r=0.49$ ), second ( $r=0.47$ ) and third ( $r=0.67$ ) terms of the WPL correction. The distortion of the E-C flux estimates by cross sensitivity to humidity is a common problem with open-path IRGA, raising substantially their detection limit. The observed differences between the concentrations of  $\text{CO}_2$  in the air and in the water during our survey varied within 120 and 270 Appm, well below the limit for a 25% error in the flux estimator as reported by Blomquist et al. (2014) for our IRGA model, the LI-COR LI 7500. We hypothesize

345 whether the E-C data lacked quality to calibrate and validate the formulations. However, our formulations were close matches to the estimates by widely used transfer velocity formulations subject to thorough calibration and validation, which proved them reasonable estimators of the central tendency (Fig. 3). Hence, we were confident about the potential of our newly proposed formulations to replicate the central tendency similarly well while improving the accuracy of the estimates for each particular location.

350 the  $k_w$  estimated from the Eddy-Covariance (E-C) measurements During this Baltic Sea sampling at the Östergarnsholm site were close matches to the  $k_w$  estimated by both generalistic and comprehensive algorithms (Fig.3). The observed differences between the concentrations of  $\text{CO}_2$  in the air and in the water during our survey varied within 120 and 270 Appm, well below the limit for a 25% error in the flux estimates as reported by Blomquist et al. (2014) for our IRGA model, the LI-COR LI 7500. The mismatches found in previous versions of this report were consequence of humidity mistakenly input in incorrect units into the E-C matlab script. The mismatches currently seen at lower wind speeds may be due to failure of the E-C measurements under atmospherically stable conditions, a problem well known to affect E-C methods. During the experiment the SBL was generally stable ( $0 < Ri_b < 0.09$ ) with a couple of few exceptions above 0.09 while the sea-surface was little to moderately rough ( $z_0 < 0.49$  mm). These conditions were used as reference to estimate the elasticity of  $k_w$  to the environmental variables its forcing functions (Fig. 4). The variables related with the SBL stability, namely the  $u_{10}$ , temperature, pressure and humidity, were the variables able to induce larger changes in  $k_w$ . However, the SBL stability changed little during this experiment whereas the sea-state change considerably, with a calmer period during which the sea-surface was smoother and a harsher period during which the sea-surface was rougher (Fig.3). Hence, during this experiment the sea-state had a greater impact on the  $k_w$  than the atmospheric stability. The  $k_w$  dependency on the sea-state is well-known as it is thought that  $k_w$  scales with the turbulent kinetic energy dissipation at the sea-surface ( $\epsilon$ ) and that this is better reflected by the sea-state (Soloviev et al., 2007, Wang et al., 2015). Accordingly, the COARE 3.0 included the wave state in the estimation of the roughness parameters essential for the transfer of mass, heat and momentum (Fairall et al. 2003) while Frew et al. (2004) observed a remarkable correlation between the  $k_w$  and small scale waves. Our comprehensive algorithms adjusted to the sea-state splitting the  $k_w$  estimates into two distinct groups relative to each period. The  $k_w$  estimated for the rougher sea-states scattered along a steeper line placed above the  $k_w$  estimated for the smoother sea-states. The  $k_w$  estimated from the E-C measurements tended to follow this same pattern (Fig.3), and episodic departure from it may be inherent to E-C natural variability. renowned  $u_{10}$ -based formulations were used and compared with the most comprehensive alternatives provided in our software and framework (Fig. 3). Although their estimates were close matches, there were a few

355

360

365

370

375 fundamental differences: the comprehensive algorithms split the data points into two distinct scatter lines, the upper line  
for  $k_w$  obtained under rougher sea surfaces and the lower line for  $k_w$  obtained under smoother ones. The red markers  
representing the ZRb03 iWLP give the best example. The generalistic  $u_{10}$ -based formulations were unable to perform  
this adjustment to the local wave state. Their small  $k_w$  fluctuations were a sole consequence of changes in water  
viscosity (as estimated by the  $Sc_w$ ) driven by changes in water temperature. Furthermore, the Wan92 formulation and  
380 our comprehensive formulations adjusted remarkably well under rougher seas, whereas the Cea96 formulation  
calibrated with data from the Parker river estuary and our comprehensive formulations adjusted remarkably well under  
lighter winds and/or smoother seas (Fig.3). These fits clearly show an ability of our comprehensive algorithms to adjust  
to the local conditions that cannot be met by the generalistic  $u_{10}$ -based formulations. This is not a minor detail: at  $u_{10} \approx 8$   
 $m \cdot s^{-1}$  the  $k_w$  estimated from wind dragging over rougher or over smoother sea-surfaces differed  $\approx 31\%$  while at  $u_{10} < 4$   
 $m \cdot s^{-1}$  the  $u_{10}$ -based formulations estimated less than 50% of the  $k_w$  estimated by our comprehensive algorithms.  
385 Furthermore, under the lowest winds the  $k_w$  estimated by  $u_{10}$ -based formulations tended to zero, with the exception of  
the formulations by McGillis et al. (2001) and Wanninkhof et al. (2009) as explained below. This is a bias from reality  
that has been thoroughly debated during the last decades. The COARE algorithm addressed it by adding a gustiness  
term to stabilize the  $k_w$  in effective velocities under lighter winds (Grachev and Fairall, 1996; Fairall et al., 2003). With  
the same objective, Clayson et al. (1996) replaced the gustiness term by a capillary wave parameterization. Mackay and  
390 Yeun (1983), McGillis et al. (2001), Wanninkhof et al. (2009) and Johnson (2010) added a constant to the  $k_w$  equation.  
In our case, due to the iWLP (equations 14 and 16) and the  $k_w$  dependence on  $u_*$ , under the lowest winds but as long as  
there are waves, our comprehensive algorithms always provide effective velocities similar to the estimated by the  
authors mentioned above. Hence, our solution resembles the solution by Clayson et al. (1996). These results highlight  
the potential of the SBL stability and the sea surface agitation as additional  $k_w$  mediators. It is curious that the wave  
395 variables were the responsible for the big differences between  $k_w$  estimates (as shown in Fig. 3) although these were the  
variables to which the  $k_w$  was least elastic (as shown in Fig. 4). It demonstrates that more important than model  
sensitivity (or elasticity) is how much the respective variables effectively change in the real world. There was yet the  
interesting detail of how the WLLP and the iWLP diverged under smoother sea-surfaces (not shown), supporting the  
solution suggested in the COARE 3.0 (Fairall et al., 2003) for the iterative estimation of  $u_*$  and  $z_0$ .

400 We performed Complementary to the analysis above, we also used the simulations of the European coastal oceans  
to compare between the ESM standard (the Wan92) and one of our comprehensive alternatives. (We show the  
comparison with the iWLP-WZRb05va3), chosen on the basis of two factors: it was both the most elastic formulation  
and the one providing the closest estimates to the Wan92 (recall Fig. 3). Since the Wan92 often represented the central  
405 tendency of the iWLP ZRb03, this choice provided the best probability that the differences between the  $k_w$  estimates  
were due to the enhanced representation of the environmental processes involved and not to systematic biases  
associated to uncertainty in the parameter estimation. Both Their  $k_w$  estimates diverged under two particular mostly  
situations (Fig. 5): (i) under low winds and unstable SBL, very rough or very smooth sea-surfaces, or higher friction  
velocities, and (ii) under high winds and rougher sea surfaces (Fig. 5). The details of the simulations and the differences  
between  $k_w$  estimates are presented hereafter.

410 Strong winds occurred along the European shores from the 24<sup>th</sup> to the 26<sup>th</sup> of May of 2014. Besides, the air was  
unusually cold for the season and colder than the sea-surface (Video 1). The upward advection rise of the warmer air,  
heated by the sea-surface, generated turbulent eddies that enhanced mixing within the SBL. These unstable conditions

were identified by  $Ri_b < 0$ ,  $L$  tending to  $\infty$  and  $\psi_m < 0$  (Video 2). The mixing of the SBL enhanced  $u_*$  and  $k_w$  everywhere the wind blew lighter. This situation occurred more frequently and intensively nearby land masses and often associated to cooler continental breezes blowing off-shore. Its correct simulation required the estimation of the  $Ri_b$ ,  $L$  and  $\psi_m$  from the algorithms by Grachev and Fairall (1997) and Stull (1988) that account for humidity considering saturation at 0 m heights. The  $Ri_b$  estimates neglecting humidity, following (Lee, (1997), often yielded neutral conditions biased estimates of the (i.e., with  $Ri_b \approx 0$ ) or unreasonably stable-SBL conditions (i.e., with  $Ri_b > 0$ ) as consequence of biased estimates of the virtual potential temperature. Stull (1988, page 9), Grachev and Fairall (1996) and Fairall et al. (2003) already highlighted the importance of accounting for humidity.

The sea-surface agitation was very heterogenic, particularly at the coastal ocean where it attained both the highest and the lowest estimated roughness lengths (the  $z_0$  in Video 3). There, the steeper waves, as a consequence of shorter fetches, should extract more momentum from the atmosphere under similar  $u_{10}$  conditions (Taylor and Yelland, 2001; Fairall et al, 2003). Thus, the rougher coastal ocean surfaces were expected to possess more turbulent layers through which gases were transferred at higher rates. The comprehensive formulations simulated this by increasing  $u_*$  (and consequently  $k_{wind}$ ) with  $z_0$  under similar  $u_z$  i.e., similar winds generate more drag when blowing over harsher sea-surfaces. Aside the rougher weather, whenever lighter wind blew over smoother sea-surfaces, the iWLP estimated much higher  $z_0$  than the WLLP (video 4), demonstrating that the smooth flow was a fundamental driver for the  $z_0$  under calmer weather. This increase in  $z_0$  lead to significantly higher  $u_*$ , often 1.5 times higher and sometimes more, anticipating a significant impact on the  $k_{wind}$  estimates.

In some rare situations the algorithms estimated unreasonably high  $k_w$  despite the  $z_0$  bounds imposed in the software. To avoid this bias, all  $k_w$  estimates were imposed a  $200 \text{ cm} \cdot \text{h}^{-1}$  ceiling.

The comprehensive formulation (i.e., WZRb053va-iWLP) often estimated  $k_w$  largely higher than and the one estimated by the ESM standard formulation (i.e., Wan92 formulations often diverged), although it occasionally estimated lower their  $k_w$  estimates, particularly in the coastal ocean, both on the Atlantic side and on the Mediterranean side, and mostly associated to storms (Video 5). Integrated over space and time, the Wan92 transferred  $33061 \text{ km}^3$  of  $\text{CO}_2$  across the  $\approx 5,054,896 \text{ km}^2$  of ocean surface during the 66 h that the experiment lasted, corresponding to 90.8% of the  $36392 \text{ km}^3$  of  $\text{CO}_2$  transferred by the W05va formulation. However, as the bias occurred in both directions the absolute bias summed to  $11880 \text{ km}^3$ . These differences were higher at the coastal ocean (Fig. 6), a consequence of the factors that were not taken into consideration by the Wan92 (the ESM standard). Apart the  $\text{CO}_2$ , the W05va transferred  $35479 \text{ km}^3$  of  $\text{CH}_4$  and of  $\text{N}_2\text{O}$ . Its largest estimates of  $k_w$  were associated to unreasonably high estimates of  $z_0$  that biased the subsequent results. These biased estimates of  $z_0$  could either be due to a poor calibration of the Taylor and Yelland (2001) model estimating  $z_0$  from the wave field or due to biased wave field provided by the WW3-NEMO. To avoid this bias,  $k_w$  was imposed a  $70 \text{ cm} \cdot \text{h}^{-1}$  ceiling, corresponding to the maximum reported in the bulk literature associated to similar wind speeds. With this restriction, the difference in the  $\text{CO}_2$  volume transferred by either formulation across the  $\approx 5,054,896 \text{ km}^2$  of ocean surface during the 66 h was of  $12997 \text{ km}^3$ , corresponding to 33.7% of the  $38551 \text{ km}^3$  of  $\text{CO}_2$  total volume transferred using the ESM standard formulation (Fig. 6). These differences were higher at the coastal ocean, a consequence of the factors that were not taken into consideration by the ESM standard. This formulation was also used to compare between the  $k_{wind}$  and  $k_{bubble}$  components of  $k_w$ . The results showed that the  $k_{bubble}$  term was always lower than the  $k_{wind}$  term and only close to it in two situations: (i) often in the fetch-unlimited Atlantic, and (ii) in a few storms inside the Atlantic where, given their high winds, fetch was not a limitation. The total

volumes of CH<sub>4</sub> and of N<sub>2</sub>O transferred were 41156 Km<sup>3</sup> and 41158 Km<sup>3</sup>, respectively. ~~Whatever the greenhouse gas,~~ the differences were negligible between estimating k<sub>w</sub> using the single layer or the double layer schemes to estimate k<sub>w</sub> (Video 5) ~~even for a rather insoluble gas as is CH<sub>4</sub> (Fig. 6 and Video 5).~~ Nevertheless, it is worth noting that it was again ~~in the fetch limited coastal ocean under the Mediterranean storms that where most of~~ the bigger differences were found for a rather insoluble gas as is CH<sub>4</sub> (Fig. 6 and Video 5).

#### 4 Discussion

The accurate estimation of the balances of greenhouse gases and aerosols in the atmosphere and in the oceans, as well as their fluxes across the surfaces of the coastal oceans, is an important issue for biogeosciences and Earth-System modelling (ESM). Previous estimates of CO<sub>2</sub> uptake by the global oceans done by coarse resolution implementations diverged in about 70 % depending on the transfer velocity formulations being used (Takahashi et al., 2002), whereas the wide uncertainty in the ocean N<sub>2</sub>O source to the atmosphere mostly originated from the uncertainty in the air-water transfer velocities (Nevison et al., 1995). However, the knowledge on this subject is still limited, with plenty of room for improvement. As an example, the simpler formulations for the estimation of k<sub>w</sub> assume either a quadratic or cubic dependency from u<sub>10</sub> depending mostly on the sensing method, time scale and fetch at the particular location. Furthermore, the simulation of atmosphere-ocean interactions by regional and Earth-system models, by still using these simpler formulations, are decades behind the state of the art. Our work proposes a framework to incorporate this state of the art in an atmosphere-ocean coupler and demonstrates that this is fundamental for reliable simulations of coastal ocean systems.

~~Remarkably, both~~ solubility formulations generally estimated similar solubilities ~~matched their estimates~~ despite their distinct chemistry backgrounds. Nevertheless, they did diverge in as much as 0.045 mol·mol<sup>-1</sup> of CO<sub>2</sub>, 0.0015 mol·mol<sup>-1</sup> of CH<sub>4</sub> and 0.012 mol·mol<sup>-1</sup> of N<sub>2</sub>O (i.e. mol of gas in the ocean surface per mol of gas in the atmosphere) in some of the most sensitive situations for Earth-System modelling and satellite data processing: (i) the cooler marine waters occur closer to the poles, where the solubility pump traps greenhouse gases and carries them to the deep ocean (Sarmiento and Gruber, 2013), and (ii) the warmer and the less saline waters occurring at the coastal ocean and seas, which have regularly been observed having greenhouse gases and DMS and aerosols dissolved in concentrations highly unbalanced with those of the atmosphere (Nevison et al., 2004; Borges et al., 2005; Barnes and Upstill-Goddard, 2011; Sarmiento and Gruber, 2013; Dutta et al., 2015; Gypens and Borges, 2015; Harley et al., 2015). Therefore, the biases in the estimated total amount of greenhouse gases in the first meter depth of the European coastal ocean during late May 2014 may be an indicator of higher global biases.

The accurate estimation of the transfer velocities of greenhouse gases and DMS across the ocean surface is a fundamental issue for biogeosciences and Earth-System modelling. Previous estimates of CO<sub>2</sub> uptake by the global oceans done by coarse resolution implementations diverged in about 70 % depending on the formulations being used (Takahashi et al., 2002), whereas the wide uncertainty in the ocean N<sub>2</sub>O source to the atmosphere mostly originated from the uncertainty in the air-water transfer velocities (Nevison et al., 1995). Despite its importance, the knowledge on this subject is still limited, with plenty of room for improvement. The simpler formulations assume either quadratic or cubic dependencies of k<sub>w</sub> from u<sub>10</sub> depending mostly on the sensing method, time scale and fetch (Wanninkhof, 1992; Nightingale et al., 2000; McGillis et al., 2001; Ho et al., 2006; Sweeney et al., 2007; Wanninkhof et al., 2009). Meanwhile, there were substantial developments on the effects of other factors as wave state, atmospheric stability,

495 ~~currents, surfactants, rain and ice cover. Our framework integrates these factors and allows comparison among~~  
~~algorithms of different degrees of complexity. Furthermore, we programmed it to automatically select simpler~~  
~~algorithms when lacking variables indispensable for the application of the more comprehensive ones. Hence, this~~  
~~framework can also be used as basis for atmosphere-ocean couplers in regional and Earth-system models. Our~~  
~~comparisons demonstrated that the more comprehensive algorithms outperform the simpler ones by taking into~~  
~~consideration factors that are fundamental for~~  
~~This work showed that the accurate estimation of the transfer velocity of greenhouse gases and aerosols/DMS across the~~  
~~coastal oceans' surface requires taking into consideration at least~~  
~~The most determinant factors were~~ the atmospheric  
500 stability of the SBL and the sea-surface roughness. ~~Similar conclusions were~~ recently ~~suggested~~~~achieved~~ by Jackson  
et al. (2012) and Shuiqing and Dongliang (2016).

~~Our results show that, by neglecting these factors, the simpler  $u_{10}$ -based formulations tend to provide lower~~  
~~estimates of the transfer velocity than the provided by comprehensive formulations. Similar conclusions were achieved~~  
~~by Jackson et al. (2012). However,~~ ~~t~~The more comprehensive formulations still need improvement and validation. It is  
505 imperative to calibrate and validate the estimation of transfer velocity ( $k_w$ ) from friction velocity ( $u_*$ ) and wind-wave  
breaking ( $k_{\text{bubble}}$ ), and the roughness length ( $z_0$ ) from the wave field. All the available formulations for these specific  
purposes lack robust parameter estimations. Generally, there seems to be a great dependency of the available algorithms  
from the particular data sets that were used to calibrate them. Nevertheless, there is a general consensus that the  $k_{\text{bubble}}$   
term is fundamental under high wind speeds, with its estimate being central to current  $k_w$  research. The latest  
developments have been on the dependency of  $k_{\text{bubble}}$  from the interactions among the wind, the wave state, the bubble  
510 plume and the properties of the gas being transferred (Woolf et al. 2007; Callaghan et al., 2008, 2014; Goddijn-Murphy  
et al., 2011, Crosswell, 2015). The effect of sea-spray ~~is the new buzz on this topic and only~~ recently ~~became a~~  
~~prominent topic with the~~~~started~~ ~~emergence of~~ algorithms like the ones by Zhao et al. (2006) and Wu et al. (2015),  
~~and a dedicated section in the latest atmosphere-ocean interactions workshop in Brest.~~ So far, these focused on the  
momentum transfer from wind to the ocean surface and the attenuation of the friction velocity. It should be interesting  
515 to understand how the intrusion of the sea-spray on the atmosphere affects the transfer velocity of gases, being  
anticipated a process symmetrical to that of the intrusion of bubbles on the ocean. The new algorithms for the effects of  
surfactants are particularly concerned with the variability of the coastal ocean (Pereira et al., 2016). These no longer  
associate the surfactants to the Schmidt number's exponent but rather to a coefficient setting a proportional decay of  $k_w$ .  
The effect of sea-ice must take into consideration its distortion of the ocean surface and its effect upon the SBL stability  
520 (Loose et al., 2014). Our coupling solution still needs to integrate the effects of the sea-surface cool-skin and warm-  
layer, surfactants, rain, sea-spray and sea-ice. From these, the cool-skin and warm-layer algorithms are the only with  
robust calibrations and validations, mostly done under the COARE (Fairall et al., 1996; Fairall et al., 2003; Zeng and  
Beljars, 2005; Brunke et al., 2008). The addition of complexity to any coupling solution must be carefully thought as  
these cannot become intricate to the point of ~~computational~~~~calculus~~ becoming unbearable for ESM application. ~~In~~  
525 ~~particular, any a~~Algorithms ~~demanding~~~~making extensive use of~~ for-loops ~~is~~are unviable: (i) ~~as~~ ~~if~~loops are  
~~computationally slow and (ii) disables~~ ~~can easily become conflictive with~~ ~~calculus~~-vectorization and its coordination  
with parallel processing. ~~Hence,~~ ~~In~~ our software ~~needed a deep restructuration from its original version presented in~~  
~~Vieira et al. (2013). Once done,~~ vectorization ~~per se~~ enabled improving calculations~~s~~ roughly 12× faster in a single  
core.

530

Besides finding the appropriate algorithms and parameter values to be used by the coupler, there is also the issue of accurately retrieving the variables mediating the gas transfer. The results showed that the  $k_w$  was most elastic to the variables related with the SBL stability, namely the  $u_{10}$ , temperature, pressure and humidity. Although these are provided by the oceanic and atmospheric model components at coarser vertical resolutions, they need to be transposed to finer vertical resolutions taking into consideration the processes occurring at the sea surface. While the  $u_{10}$  is given by the atmospheric model, the water temperature needs to account for the cool skin and warm layer effects and the heat and humidity at the SBL need to account for their vertical fluxes over the sea surface. The COARE algorithm is the state-of-the-art in the estimation of atmosphere-open ocean fluxes for these tasks. During most of its development it focused on E-C methods to the estimation of the fluxes of the heat and humidity across the SBL fluxes using a framework with an intricate mathematical structure going deeper into the simulation of the geophysical process. Only in its latter developments did the COARE explicitly address the gas fluxes of gases and the importance of sea surface roughness (Fairall et al. 2003; Jeffrey et al., 2010; Blomquist et al., 2006, 2014; Jeffrey et al., 2010). Given Unfortunately, its complexity is deterrent of application to already computationally intensive geoscientific models. The transferred quantities of heat, moisture and momentum, their transfer coefficients, the dimensionless roughness lengths and the gustiness term are interdependent and must be solved iteratively. The COARE estimation of the  $w_m$  alone is computationally heavier than the most comprehensive ensemble possible in the FuGas 2.2. The COARE was recently introduced as optional in the MOHID model and software. Our preliminary trials testing the heat transfer took  $\approx 14\%$  longer to run each simulation.

535

540

545

550

~~it must be quite a challenge to perform the calculus vectorization and parallelization required for the substantial improvement of computational speed and its application to ESM. Only in its latter developments did the COARE explicitly address the fluxes of gases and the importance of sea surface roughness (Fairall et al., 2003; Jeffrey et al., 2010; Blomquist et al., 2006, 2014).~~

## 5 Code and Data Availability

555

Software and data related to this article provided as supplementary material. Software, data and videos related to this article available at <http://www.maretec.org/en/models/fugas>

## 6 Acknowledgments:

560

To windguru.cz for the support providing the wave data. Work funded by ERDF Funds of the Competitiveness Factors Operational Programme - COMPETE and by national funds from the FCT - Foundation for Science and Technology project UID/EEA/50009/2013.

## 7 References

565

- Asher, W. E. and Farley, P. J.: Phase-Doppler anemometer measurement of bubble concentrations in laboratory-simulated breaking waves, J. Geophys. Res., 100C: 7045-7056, 1995.
- Barnes, J. and Upstill-Goddard, R. C.: N<sub>2</sub>O seasonal distributions and air-sea exchange in UK estuaries: implications for the tropospheric N<sub>2</sub>O source from European coastal waters. J. Geophys. Res. 116, G01006, 2011.

- 570 Blomquist, B. W., Fairall, C. W., Huebert, B. J., Kieber, D. J. and Westby, G. R.: DMS sea-air transfer velocity: Direct measurements by eddy covariance and parameterization based on the NOAA/COARE gas transfer model. *Geophys. Res. Lett.*, 33(7), L07601, doi:10.1029/2006GL025735, 2006.
- Blomquist, B. W., Huebert, B. J., Fairall, C. W., Bariteau, L., Edson, J. B., Hare, J. E. and McGillis, W. R.: Advances in Air–Sea CO<sub>2</sub> Flux Measurement by Eddy Correlation. *Boundary-Layer Meteorology*, 152(3):245–276, 2014.
- 575 Borges, A. V., Vanderborght, J. P., Schiettecatte, L. S., Gazeau, F., Ferron-Smith, S., Delille, B. and Frankignoulle, M.: Variability of the Gas Transfer Velocity of CO<sub>2</sub> in a Macrotidal Estuary (the Scheldt), *Estuaries*, 27, 593–603, 2004.
- Borges, A.V., Delille, B., and Frankignoulle, M.. Budgeting sinks and sources of CO<sub>2</sub> in the coastal ocean: Diversity of ecosystems counts, *Geophys. Res. Lett.*, 32, L14601, doi:10.1029/2005GL023053, 2005.
- 580 Brunke, M. A, Zeng, X., Misra, V. and Beljaars, A.: Integration of a prognostic sea surface skin temperature scheme into weather and climate models. *J. Geophys Res.*, 113, D21117, doi: 10.1029/2008JD010607, 2008.
- Callaghan, A. H., Deane, G. B. and Stokes, M. D.: Observed physical and environmental causes of scatter in whitecap coverage values in a fetch-limited coastal zone. *J. Geophys. Res.*, 113(C5), 10.1029/2007JC004453, 2008.
- Callaghan, A. H., Stokes, M. D. and Deane, G. B.: The effect of water temperature on air entrainment, bubble plumes, and surface foam in a laboratory breaking-wave analog. *J. Geophys. Res.*, 1193(CS11), [10.1029/2007JC004453](https://doi.org/10.1029/2007JC004453), 201408.
- 585 Carini, S., Weston, N., Hopkinson, C., Tucker, J., Giblin, A., and Vallino, J.: Gas exchange rates in the Parker River estuary, Massachusetts. *Biol. Bull.*, 191, 333–334, 1996.
- Clayson, C. A., Fairall, C. W. and Curry, J. A.: Evaluation of turbulent fluxes at the ocean surface using surface renewal theory. *J. Geophys. Res.*, 101, 28503–28513, 1996.
- 590 Clementi E., Oddo P., Korres G., Drudi M. and Pinardi N.: Coupled wave-ocean modelling system in the Mediterranean Sea. Extended abstract to the 13th Int. Workshop on Wave Hindcasting, Banff, Canada, 2013.
- Crosswell, J. R.: Bubble clouds in coastal waters and their role in air-water gas exchange of CO<sub>2</sub>. *J. Mar. Sci. Eng.*, 3, 866-890; doi:10.3390/jmse3030866, 2015.
- 595 Dutta, M. K., Mukherjee, R., Jana, T. K. and Mukhopadhyay, S. K.: Biogeochemical dynamics of exogenous methane in an estuary associated to a mangrove biosphere; The Sundarbans, NE coast of India. *Mar. Chem.*, 170, 1-10, 2015.
- EPA United States Environmental Protection Agency - Climate Change Indicators in the United States - Atmospheric concentrations of greenhouse gases, <http://www.epa.gov/climatechange/science/indicators/ghg/ghg-concentrations.html>, last accessed: 27 August 2015.
- 600 Fairall, C.W., Bradley, E. F., Godfrey, J. S., Wick G. A., Edson, J. B. and Young G. S.: Cool-skin and warm-layer effects on sea surface temperature, *J. Geophys. Res.*, 101, 1295–1308, 1996.
- Fairall, C. W., Bradley, E.F., Hare, J.E., Grachev, A.A., and Edson, J.B.: Bulk parameterization of air-sea fluxes: updates and verification for the COARE algorithm, *J. Climate*, 16, 571–591, 2003.
- 605 Goddijn-Murphy, L., Woolf, D. K. and Callaghan, A. H.: Parameterizations and Algorithms for Oceanic Whitecap Coverage. *Journal of Physical Oceanography*, 41, 742-756, 2011.



- Grachev, A. A. and Fairall, C. W.: Dependence of the Monin–Obukhov Stability Parameter on the Bulk Richardson Number over the Ocean. *J. Appl. Meteorol.*, 36, 406–414, 1997.
- Gypens, N. and Borges, A. V.: Increase in dimethylsulfide (DMS) emissions due to eutrophication of coastal waters offsets their reduction due to ocean acidification, *Front. Mar. Sci.*, 1, 4. doi: 10.3389/fmars.2014.00004, 2015.
- 610 Harley, J. F., Carvalho, L., Dudley, B., Heal, K. V., Rees, R. M. and Skiba, U.: Spatial and seasonal fluxes of the greenhouse gases N<sub>2</sub>O, CO<sub>2</sub> and CH<sub>4</sub> in a UK macrotidal estuary, *Estuar. Coast. Shelf S.*, 153, 62, 2015.
- [Ho, D. T., Law, C. S., Smith, M. J., Schlosser, P., Harvey, M. and Hill, P.: Measurements of air-sea gas exchange at high wind speeds in the Southern Ocean: Implications for global parameterizations, \*Geophys. Res. Lett.\*, 33, L16611, doi:10.1029/2006GL026817, 2006.](#)
- 615 [Högström, U., Sahlée, E., Drennan, W. M. Kahma, K. K., Smedman, A.-S., Johansson, C., Pettersson, H., Rutgersson, A., Tuomi, L, Zhang, F. and Johansson, M.: To what extent can we believe measurements on a land-based tower to represent upwind open sea conditions? \*Boreal Environ. Res.\*, 13, 475-502, 2008.](#)
- Jackson, D. L., Wick, G. A. and Hare, J. E.: A comparison of satellite-derived carbon dioxide transfer velocities from a physically based model with GasEx cruise observations. *J. Geophys. Res.* 117, G00F13, doi:10.1029/2011JC007329, 2012.
- 620 Jähne, B., Munnich, K. O., Bosinger, R., Dutzi, A., Huber, W. and Libner, P.: On the parameters influencing air-water gas exchange. *J. Geophys. Res.*, 92, 1937–1949, 1987.
- Jeffery, C., Robinson, I., and Woolf, D.: Tuning a physically-based model of the air-sea gas transfer velocity, *Ocean Modell.*, 31, 28–35. doi:10.1016/j.ocemod.2009.09.001, 2010.
- 625 Johnson, M. T.: A numerical scheme to calculate temperature and salinity dependent air-water transfer velocities for any gas, *Ocean Sci.*, 6, 913–932, 2010.
- Lee, H.N.: Improvement of surface flux calculations in the atmospheric surface layer, *J. Appl. Meteorol.*, 36, 1416–1423, 1997.
- 630 Liss, P. S. and Slater, P. G.: Flux of gases across the air-sea interface, *Nature*, 247, 181–184, 1974.
- Loose, B., McGillis, W. R., Perovich, D. Zappa, C. J. and Schlosser, P.: A parameter model of gas exchange for the seasonal sea ice zone, *Ocean Sci.*, 10, 17–28, 2014.
- [McGillis, W. R., Edson, J. B., Ware, J. D., Dacey, J. W. H., Hare, J. E., Fairall, C. W., and Wanninkhof, R.: Carbon dioxide flux techniques performed during GasEx-98, \*Mar. Chem.\*, 75, 267–280. doi:10.1016/S0304-4203\(01\)00042-1, 2001.](#)
- 635 [Monin, A. S. and Obukhov, A. M.: Basic laws of turbulent mixing in the surface layer of the atmosphere. Translation by McNaughton, K. available at \[http://mcnaughty.com/keith/papers/Monin\\\_and\\\_Obukhov\\\_1954.pdf\]\(http://mcnaughty.com/keith/papers/Monin\_and\_Obukhov\_1954.pdf\) \(last access: 22 December 2016\), 1954.](#)
- Nevison, C. D., Weiss, R. F., and Erickson III, D. J.: Global oceanic emissions of nitrous oxide, *J. Geophys. Res.*, 100, 15809–15820, 1995.
- 640 Nevison, C. D., Lueker, T. J. and Weiss, R. F.: Quantifying the nitrous oxide source from coastal upwelling, *Global Biogeochem. Cy.*, 18, GB1018, doi:10.1029/2003GB002110, 2004.
- [Nightingale, P. D., Malin, G., Law, C. S., Watson, A. J., Liss, P. S., Liddicoat, M. I., Boutin, J., and Upstill-Goddard, R. C.: In Situ Evaluation of Air-Sea Gas Exchange Parameterizations Using Novel Conservative and Volatile Tracers, \*Global Biogeocheml Cy.\*, 14, 373–387, 2000.](#)
- 645

- OCMIP: Ocean Carbon-Cycle Model Intercomparison Project, available at: <http://ocmip5.ipsl.jussieu.fr/OCMIP>, last updated: 2004 (last access: 27 August 2015), 2004.
- Pereira, R., Scheneider-Zapp, K. and Upstill-Goddard, R.: Surfactant control of gas transfer velocity along an off-shore coastal transect: results from a laboratory gas exchange tank, *Biogeosciences Discuss.*, doi:10.5194/bg-2016-7, 2016.
- 650 Raymond, P. A. and Cole, J. J.: Gas exchange in rivers and estuaries: choosing a gas transfer velocity, *Estuaries*, 24, 312–317, 2001.
- Rutgersson, A., Norman, M., Schneider, B., Petterson, H. and Sahlée, E.: The annual cycle of carbon dioxide and parameters influencing the air–sea carbon exchange in the Baltic Proper, *J. Marine Sys.*, 74: 381-394, 2008.
- 655 Sander, R.: Compilation of Henry's law constants (version 4.0) for water as solvent, *Atmos. Chem. Phys.*, 15, 4399-4981, doi:10.5194/acp-15-4399-2015, 2015.
- Sarmiento, J. L. and Gruber, N.: *Ocean Biogeochemical Dynamics*. Princeton University Press, New Jersey, USA. pp73-100, 2013.
- Shuiqing, L. and Dongliang, Z.: Gas transfer velocity in the presence of wave breaking. *Tellus B*, 68, 27034, 2016.
- 660 [Soloviev, A., Donelan, M., Graber, H., Haus, B. and Schlüssel, P.: An approach to estimation of near-surface turbulence and CO2 transfer velocity from remote sensing data, \*J. Mar. Sys.\*, 66, 182-194, 2007.](#)
- Stull, R. B.: An introduction to Boundary Layer Meteorology, Kluwer Academic Publishers, Dordrecht, pp151-195, 1988.
- 665 [Sweeney, C., Gloor, E., Jacobson, A. R., Key, R. M., McKinley, G., Sarmiento, J. L. and Wanninkhof, R.: Constraining global air-sea gas exchange for CO2 with recent bomb <sup>14</sup>C measurements, \*Global Biogeochem. Cy.\*, 21, GB2015, doi:10.1029/2006GB002784, 2007.](#)
- Takahashi, T., Sutherland, S. C., Sweeney, C., Poisson, A., Metzl, N., Tilbrook, B., Bates, N., Wanninkhof, R., Feely, R. A., Sabine, C., Olafsson, J., and Nojirih, Y.: Global sea–air CO2 flux based on climatological surface ocean pCO<sub>2</sub>, and seasonal biological and temperature effects, *Deep-Sea Res.*, 49, 1601–1622, 2002.
- 670 Taylor, P. K. and Yelland, M. J.: The dependence of sea surface roughness on the height and steepness of the waves, *J. Phys. Oceanogr.*, 31, 572–590. 2001.
- Vieira, V. M. N. C. S., Martins, F., Silva, J. and Santos, R.: Numerical tools to estimate the flux of a gas across the air–water interface and assess the heterogeneity of its forcing functions. *Ocean Sci.*, 9, 355-375, 2013.
- 675 [Wang, B., Liao, Q., Fillingham, J. and Bootsma, H. A.: On the coefficients of small eddy and surface divergence models for the air-water gas transfer velocity, \*J. Geophys. Res. Oceans\*, 120\(3\), DOI: 10.1002/2014JC010253, 2015.](#)
- Wanninkhof, R.: Relationship between wind speed and gas exchange over the ocean, *J. Geophys. Res.*, 97, 7373–7382, 1992.
- 680 [Wanninkhof, R., Asher, W. E., Ho, D. T., Sweeney, C. S., and McGillis, W. R.: Advances in quantifying air-sea gas exchange and environmental forcing, \*Ann. Rev. Mar. Sci.\*, 1, 213–244, doi:10.1146/annurev.marine.010908.163742, 2009.](#)

685 Webb, E. K., Pearman, G. I. and Leuning, R.: Correction of flux measurements for density effects due to heat and water vapour transfer. *Quart. J.R. Meteorol. Soc.*, 106: 85-100, 1980.

Weiss, R. F.: Carbon dioxide in water and seawater: the solubility of a non-ideal gas. *Mar. Chem.*, 2, 203-215, 1974.

Weiss, R. F. and Price B. A.: Nitrous oxide solubility in water and seawater. *Mar. Chem.*, 8, 347-359, 1980.

690 Woolf, D. K.: Parameterization of gas transfer velocities and sea state-dependent wave breaking. *Tellus B*, 57, 87 – 94, 2005.

Woolf, D. K., Leifer, I. Nightingale, P.D., Andreae, M.O.: Modelling of bubble-mediated gas transfer: Fundamental principles and a laboratory test. *J. Mar. Sys.*, doi: 10.1016/j.jmarsys.2006.02.011, 2007.

Wu, L., Rutgersson, A. and Sahlée, E.: The impact of waves and sea-spray on modelling storm track and development. *Tellus A*, 67, 27967, 2015.

695 Zeng, X. and Beljaars, A.: A prognostic scheme of sea surface skin temperature for modelling and data assimilation. *Geophys. Res. Lett.*, 32, L14605, 2005.

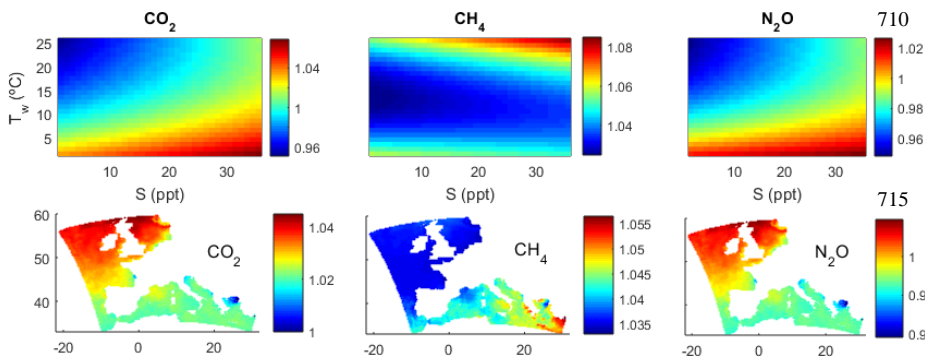
Zhang, W., Perrie, W. and Vagle, S.: Impacts of winter storms on air-sea gas exchange. *Geophys. Res. Lett.*, 33, L14803, 2006.

700 Zhao, D., Toba, Y., Suzuki, Y., and Komori, S.: Effect of wind waves on air-sea gas exchange: proposal of an overall CO<sub>2</sub> transfer velocity formula as a function of breaking-wave parameter, *Tellus B*, 55, 478–487, 2003.

Zhao, D., Toba, Y., Sugioka, K. and Komori, S.: New sea spray generation function for spume droplets. *J. Geophys. Res.*, 111(C2), doi: 10.1029/2005JC002960, 2006.

705

**8 Figures**



720 **Figure 1: Comparing solubility formulations**

725

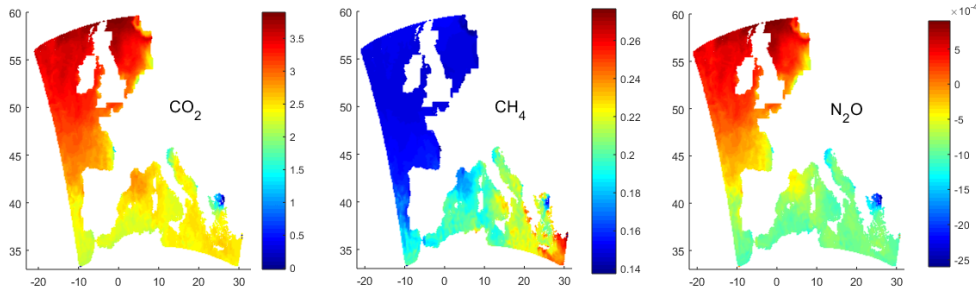


Figure 2: Bias in the gas mass balance for the European coastal ocean

730

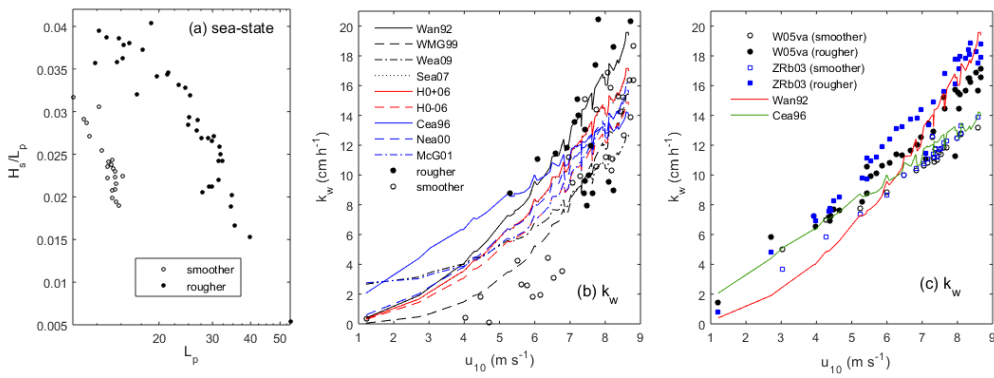


Figure 3: Comparing transfer velocity algorithms using the data observed at the Baltic.

**observed data**

735

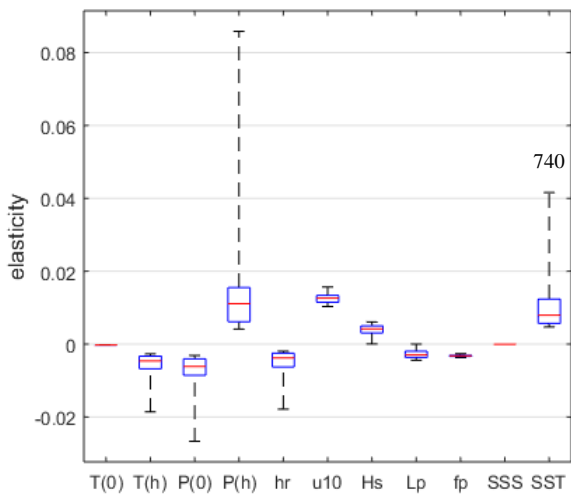
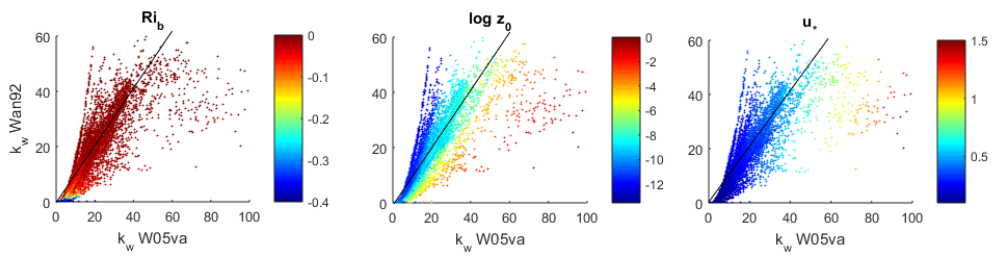


Figure 4: Elasticities of the transfer velocity to the environmental variables its forcing functions.

745

750



755

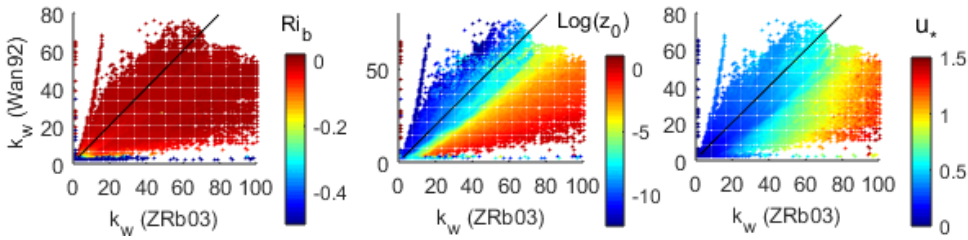


Figure 5: Applying the modelled data about the European coastal ocean for a direct comparison between the  $k_w$  estimates.

760

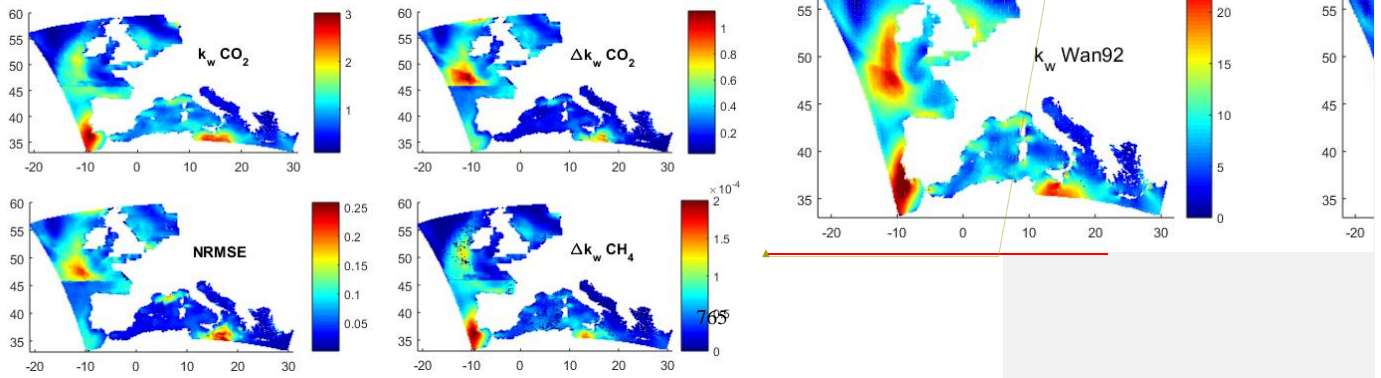


Figure 6: Comparing transfer velocity algorithms using modelled data

770

## 9 Figure legends

775

**Figure 1: Comparing solubility formulations:** match-mismatch between formulations estimating solubilities of the greenhouse gases CO<sub>2</sub>, CH<sub>4</sub> and N<sub>2</sub>O according to water temperature (T<sub>w</sub>), salinity (S) and location. Colorscale is (k<sub>H</sub>) Henry's constant estimated from (Joh10) Johnson, 2010, or (Sar13) Sarmiento and Gruber, 2013. Colorscale: quotient between k<sub>H</sub> estimated from Johnson, 2010 (k<sub>H</sub>:Joh10) and k<sub>H</sub> estimated from Sarmiento and Gruber, 2013 (k<sub>H</sub>:Sar13) i.e. k<sub>H</sub>:Joh10/k<sub>H</sub>:Sar13.

780

**Figure 2: Bias in the gas mass balance for the European coastal ocean:** comparing algorithm by Johnson (2010) to compilation by Sarmiento and Gruber (2013). Colorscale: Δton · m<sup>-1</sup> · 121 km<sup>2</sup> i.e. bias in the gas mass estimated by each algorithm (Δton) for the first meter depth (m<sup>-1</sup>) in 11 km wide cells (121 km<sup>2</sup>).

785

**Figure 3: Comparing transfer velocity algorithms using the data observed at the Baltic.** (a) sea-surface roughness given by significant wave height (H<sub>s</sub>) and peak wave period (L<sub>p</sub>). (b) The k<sub>w</sub> estimated by ~~renowned~~ u<sub>10</sub>-based formulations (lines) and by some of the most comprehensive alternatives provided in the FuGas 2.1, using compared to the k<sub>w</sub> estimated ~~data~~ from the Eddy-Covariance measurements (circles) observed at the Baltic. (c) comparing the k<sub>w</sub> estimated by u<sub>10</sub>-based formulations (lines) and by comprehensive alternatives (circles). Simple formulations by 'Wan92' - Wanninkhof (1992), 'WMG99' - Wanninkhof and McGillis (1999), 'We09' - Wanninkhof et al. (2009), 'Sea07' - Sweeney et al. (2007), 'Nea00' - Nightingale et al. (2000), 'McG01' - McGillis et al. (2001), 'Ho+06' - upper boundary in Ho et al. (2006) 'Ho-06' - lower boundary in Ho et al. (2006). Comprehensive formulations were assembled using the 'iWLP' - iteratively estimated wind log-linear profile and included the 'Jea87' - Jähne et al

790

795 (1987), ~~'Zhg06' - Zhang et al. (2006), 'ZRb03' - Zhao et al (2003), and 'W05av' - Woolf (2005) with the kinematic~~  
~~viscosity of air,~~  
~~assembled using the 'WLLP' - wind log-linear profile or the 'iWLP' - iteratively estimated wind log-linear profile.~~

800 **Figure 4: Elasticities of the transfer velocity to the environmental variables ~~its forcing functions~~. Elasticities**  
**( $\partial k_w/k_w$ )/( $\partial x/x$ ) estimated using the data observed at the Baltic. The  $k_w$  was estimated by the iterative wind log-linear**  
**profile (iWLP) with the Zhao et al (2003)  $k_{bubble}$  term (ZRb03) for the 60 observations in the Baltic. The box-and-**  
**wiskers represent the quartiles.**

805 **Figure 5: Applying the modelled data about the European coastal ocean for a direct comparison between the  $k_w$**   
**estimates by the ESM standard Wan92 - and our best performing a comprehensive formulation - W05va - including**  
**the  $k_{bubble}$  term by Woolf (2005), the  $k_{wind}$  term by Jahne et al. (1987), the  $z_0$  term from the COARE 3.0 and the iterative**  
**wind log-linear profile. The  $z_0$  is given in m and the  $u_*$  in  $m \cdot s^{-1}$ .**

810 **Figure 6: Comparing transfer velocity algorithms using modelled data: ( $k_w$   $CO_2$  Wan92) transfer velocity of  $CO_2$**   
**estimated from the formulation by Wanninkhof (1992) and averaged over the 66 h; by the 'iWLP' - iterative Wind Log-**  
**Linear Profile and the 'ZRb03' - Zhao et al. (2003) formulation, ( $\Delta k_w$   $CO_2$ ) difference between the iWLP with ZRb03**  
**and the Wan92' - Wanninkhof (1992) formulation, (NRMSE) Normalize-Root Mean Square Error between estimating**  
**the transfer velocity using the formulation by Wanninkhof (1992) or the formulation by Woolf (2005) conjugated with**  
**the iterative wind log-linear profile, iWLP with ZRb03 and the Wan92, ( $\Delta k_w$   $CH_4$ ) difference between the single and**  
**double layer schemes using the iWLP with ZRb03. Colour scale: volume (or  $\Delta$  volume) transferred in units of**  
815  **$Km^3/66h$ , except for NRMSE.**